

RETRIEVAL OF SOIL EROSION RELEVANT PARAMETERS IN THE WESTERN AUSTRALIAN WHEATBELT REGION FROM VNIR-SWIR AND TIR SPECTRAL SIGNATURES

Andreas Eisele¹, Sabine Chabrillat¹, Ian Lau², Chiaki Kobayashi³, Buddy Wheaton⁴, Dan Carter⁴, Osamu Kashimura³, Masatane Kato³, Cindy Ong², Robert Hewson², Thomas Cudahy², Hermann Kaufmann¹

¹ GFZ German Research Centre for Geosciences, Potsdam, Germany

² CSIRO, Earth Science and Resource Engineering, Perth, Australia

³ ERSDAC, Earth Remote Sensing Data Analysis Center, Tokyo, Japan

⁴ DAFWA, Department of Agriculture and Food of Western Australia

Abstract – With the focus on new available hyperspectral imaging sensors sensitive within the thermal infrared (TIR) wavelength region, this study is testing the ability of the TIR in deriving soil erosion relevant parameters (*e.g.* texture, organic carbon content) from soil spectral measurements with the respect to commonly used VNIR-SWIR spectrometers. Therefore a study site was chosen located within an agricultural area in Western Australia, which is suffering from soil loss through wind erosion processes. VNIR-SWIR and TIR soil spectra derived from laboratory measurements using common field instruments were therefore resampled to imaging sensor spectral specifications (HyMAP and TASI-600). Prediction models have been established via multivariate regression analysis techniques to quantitatively estimate the soils' physical-chemical parameters using signatures from different spectral regions.

Keywords: Thermal infrared (TIR), soil loss, texture, organic carbon

1.0 INTRODUCTION

Soil loss, acknowledged for negatively affecting paddock yield and profit, is a worldwide concern due to a reduction in surface soil fertility. This is especially true for farmers working on arid and semi-arid lands exposed to pressure through intensified land use and/or changing environmental conditions. Farming in the Western Australian wheatbelt area is dealing with such limitations because of its susceptibility to wind erosion. During the hot dry summer, strong winds blow across soils with desiccated surface layers. These surface layers, which are dominated by sandy soils, suffer from reduced stability qualities. Low in cementing agents, such as clay and soil organic matter, these fine particles are also carrying the soils' fertility potential, but have poor abilities to resist abrasion and so can easily be eroded by wind (Brady and Weil, 2008).

An assessment of the paddock's susceptibility to soil erosion, as well as the observation of the paddock's erosive progress could provide farmers and land managers with a database to recommend actions to combat soil loss in an operative way. Thus, there is a need for large-scale measurement, mapping and monitoring of surface parameters, such as the soils' surface grain size distribution and soil organic carbon content.

The use of hyperspectral techniques to quantify essential pedogenic surface parameters is attractive for soil scientists due to the reduction in the need for time- and cost-intensive soil laboratory analyses and field campaigns (Ben-Dor *et al.*, 1999). Several studies have demonstrated that such soil characteristics can be

quantified and predicted statistically via their spectral signatures in the commonly used/accessible visible to shortwave infrared (0.4 to 2.5 μm) wavelength region (Bartholomeus *et al.*, 2008; Viscarra Rossel *et al.*, 2006; Chabrillat *et al.*, 2002; Chang and Laird, 2002). This issue was addressed through a joint venture, comprising the expertise of Australian partners from Commonwealth Scientific and Industrial Research Organization (CSIRO) and the Department of Agriculture and Food of Western Australia (DAFWA), Japanese partners from the Earth Remote Sensing Data Analysis Center (ERSDAC), and the German Research Centre for Geoscience. Working together on the test area in the Mullewa district, which is located within Western Australia's wheatbelt region, we focused on a research project on agricultural issues. Soil surface properties such as soil texture and organic carbon content, all known for being crucial players controlling the extent of soil surface loss, were quantified and predicted via their spectral signatures from multivariate regression analysis techniques. To meet the objectives, high-dimensional spectral surface data were collected during the dry season (February 2010) throughout a simultaneous field- and airborne-campaign within the investigated area. Thereby, almost 150 soil samples (not all of them are analyzed so far) were collected and spectrally measured under controlled laboratory conditions, both in the Visible to Near Infrared (VNIR)-Shortwave Infrared (SWIR) and TIR spectral regions. Also VNIR-SWIR hyperspectral airborne data was recorded with the HyMap (www.hyvista.com) spectral imager to later apply the derived prediction models on a large scale basis (in a subsequent study). Another airborne hyperspectral imaging over-flight is planned to acquire

data in the thermal infrared spectral region once the instrument is completed (Thermal Airborne Spectrographic Imager TASI-600, www.itres.com). To test the ability to quantify and predict soil surface properties from high spectral resolution remote sensing data, the multivariate statistical analyses were performed on spectral signatures, resampled to typical imaging sensor spectral specifications (HyMap and TASI-600).

The thermal infrared wavelength region reveals promising capacities for that topic, since the strongest of the silicate fundamental molecular vibration bands (reststrahlen bands of the Si-O stretching) occur in the 8-14 microns atmospheric window (Salisbury and D'Aria, 1992; Cudahy, 2000). The dominance of sandy surfaced soils in the investigation area, with quartz as their major component, which influences soil texture characteristics, points to the TIR being at least a good alternative to the VNIR-SWIR region. A combination of both regions however, including the spectral contrast power for minerals having OH- and Si-O- bonds, might even have advantages in describing soil texture characteristics.

In our presentation, we will discuss our joint research concept and present preliminary results using multivariate prediction models to quantify soil parameters from the VNIR-SWIR, the TIR and from a combination of both spectral regions.

2. METHODS

Study area

The study area is located in the semi-arid wheatbelt region of Western Australia close to the provincial town of Mullewa, which is around 380 km north of Perth. The region's climate is characterized by mildly wet winters and hot dry summers and was classified as Dry Warm Mediterranean by Beard (1976). Located geologically within the Perth Basin (the town of Mullewa is on the Yilgarn Craton, however the sample sites chosen for this study are within the Perth Basin), the area is dominated by an undulating sand plain system, which involves yellow and red sands and an alluvial valley system with relict red loams over a red-brown hardpan, which key out as Tenosols and Kandosols in the Australian Soil Classification (Isbell, 1996), respectively.

Soil sampling and analyses

Within an area of approximately 360 km² a selection of soil samples, scraped from the upper 10 mm surface, were collected during a field campaign in February 2010. Each sample is a representative of a plot area surrounded by a 7.5 metres radius circle. Some additional samples were collected further south of the area, where grey sands (Tenosols) and alkaline clays (Vertosols) were sampled to stretch the variance in soil characteristics. Based on qualitative X-ray diffraction results, the mineralogy of the samples show that the soils are quartz dominated with minor kaolinite, feldspar and smectite, as well as traces of iron oxides and calcite.

So far 89 of 150 soil samples were analysed and used in this study. The soil samples were air dried and then homogenised through a 1 mm sieve. Grain size distribution was defined by using standard pipette method following Stokes law (Mc Kenzie *et al.*, 2002.)

Soil spectral measurements

Soil reflectance in the VNIR-SWIR spectral region was measured in the laboratory on the homogenised samples using an ASD FieldSpec-Pro spectrometer with a contact probe (GFOV~10mm) in the range from 350- to 2500-nm. Spectral resolution is 3-4 nm in the 350- to 1000-nm region (spectral sampling 1.4 nm), and 10-12 nm in the 1000- to 2500-nm region (spectral sampling 2 nm). The entire spectrum is resampled at 1 nm for display purposes, which resulted in 2151 spectral bands.

Soil radiance spectra in the TIR region were recorded indoors using a micro Fourier Transform Interferometer (μ FTIR) (model 102, D&P instruments) covering the spectral range from 7 to 14 μ m with a resolution of 6 cm⁻¹ on a 4.5° (GFOV~20mm) field of view. The measurements were performed on identical soil sample surfaces for the TIR and VNIR-SWIR recordings.

The samples were preheated (60°C) to relatively suppress interfering background radiance. The instrument was regularly calibrated using a blackbody (model 41P, D&P instruments) and the background temperature. Radiance was converted to emissivity signatures using a Planck curve fitting algorithm (Green, A., pers. comm.). Bands between 7 and 7.630 μ m were excluded from the spectral range due to extreme noise levels, resulting in 208 spectral bands for analysis.

To reduce data dimensionality and with the future focus of applying the resulting models to a following hyperspectral imagery study, the spectra were resampled to imagery sensor spectral specifications. ASD spectra were resampled to HyMap spectral characteristics (125 bands with a spectral resolution of 15-20 nm and a spectral range from 450- to 2480-nm). Thereby for bands affected by atmospheric water vapor (1338 – 1498 nm and 1801 – 2008 nm) absorbance were excluded from the spectral dataset. Thus, 111 bands for the VNIR-SWIR wavelength region remain. The μ FTIR thermal infrared spectra were resampled to the TASI-600 specifications (32 bands with a spectral resolution of 109.5 nm and a spectral range from 8 to 11.5 microns). The TIR spectra were brought to reflectance using Kirchhoff's law (Nicodemus, 1965) for all the further analyses.

Model construction

To enhance spectral features some of the common spectroscopic pre-processing techniques have been applied on the spectra (Viscarra Rossel, 2008; Chang and Laird, 2002). The soil spectra were transformed from reflectance (R) to absorbance ($\log_{10}(1/R)$) and also were mean centered.

Dealing with numerous, potentially correlated predictor variables from relatively few observations, is a typical challenge in spectroscopy. Ordinary multiple regression is no longer practical in this case, due to multicollinearities. To control such associated overlapping features and difficult to interpret overtones, Partial Least Square Regression analysis PLSR (Martens and Naes, 1989) was used to relate the spectral information with the soil parameters. Leave-one-out cross-validation was performed for validation and was used to determine the optimum number of factors (f) for the prediction models. To evaluate the prediction ability of the PLSR models the following statistical parameters were used. The coefficient of determination (R^2) and the adjusted coefficient of determination (R^2_{adj}) to estimate the quality of fit and the models' predictive ability, respectively. The root mean square error of calibration (RMSEC) and the root mean square error of prediction (RMSEP) were used as a measure for the error in the calibration and the expected prediction error from the cross-validation, respectively. Additionally, the explained X-variance and Y-variance of the models were specified.

3. RESULTS AND DISCUSSION

Soil Analyses

The soil texture analyses resulted in four fractions: clay (<2 μm), silt (2 - 20 μm), fine sand (20 - 200 μm), and coarse sand (200 μm - 2000 μm), whereas clay and subsumed sand (20 - 2000 μm) were used for the modeling. Soil organic matter content (SOM) was measured using the Walkley Black method (Walkley and Black, 1934). Clay ranges were from 3.8 % to 68.4 %, silt from 0.01 to 67.1 %, and subsumed sand from 14.3 % to 96.1 %. Organic carbon ranges were from 0.05 % to 1.68 %.

Interpretation of the soil spectra

The measured spectra show absorption features typical for soils from semi-arid regions (Eisele *et al.*, 2007). Figure 1 displays a selection of the VNIR-SWIR (ASD full range) soil reflectance spectra showing their shape variations. All of the soil spectra show the common clay feature in the SWIR (close to 2.2 microns) and the common iron-oxide features in the VNIR (around 0.5 and 0.9 microns) wavelength region (Clark *et al.*, 1993).

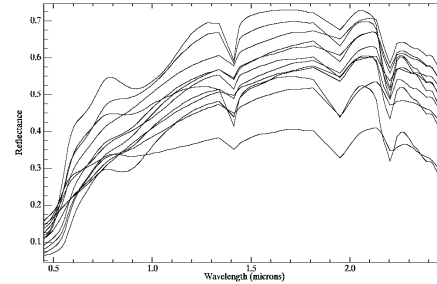


Figure 1: Selection of soil reflectance spectra in the VNIR-SWIR wavelength region (ASD full range)

Figure 2 shows reflectance spectra in the TIR (μFTIR full range) wavelength region for the same selection of soil samples as in Figure 1. The thermal infrared soil spectra clearly show the sandy character among the soil samples. Quartz, as their dominant mineral, displays the strongest of the reststrahlen bands in the thermal infrared region of any of the silicate minerals (Salisbury *et al.*, 1992), producing a principal Christiansen feature from 8- to 9.5-microns with a triple feature in between, and a secondary Christiansen feature from 12.4- to 13-microns, containing a double feature.

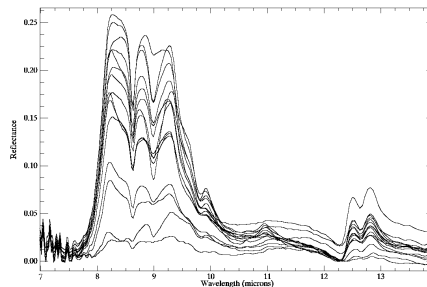


Figure 2: Selection of soil reflectance spectra in the thermal infrared wavelength region (μFTIR full range)

All of the measured soil spectra show two reflective minima (emissivity maxima) just left of the prominent Christiansen features at around 7.4 and 12.3 microns, due to the strong Si-O molecular vibration bands. Since, the TIR signatures were resampled to TASI spectral range from 8 to 11.5 microns for the prediction models, these regions will not be discussed further. Figure 3 and figure 4 show the spectral resampled (HyMap and TASI-600, respectively) and transformed (to $\log_{10}(1/R)$) soil spectra as input to the prediction modeling. As shown in both figures, the VNIR-SWIR and the TIR spectra still contain most of the original variance in wavelength after resampling.

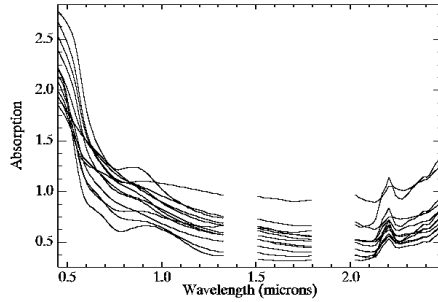


Figure 3: Selection of resampled (HyMAP) and transformed ($\log_{10}(1/R)$) soil reflectance spectra in the VNIR-SWIR as they found input to the calibration modeling

Calibration and validation of the prediction models

Calibration and validation were performed for the selected soil-erosion relevant parameters (% clay, % sand, and % organic carbon) as the response variables using the absorption spectra of the VNIR-SWIR, the TIR, and the VNIR and SWIR individually as predictors for the model. The results are summarised in Table 1.

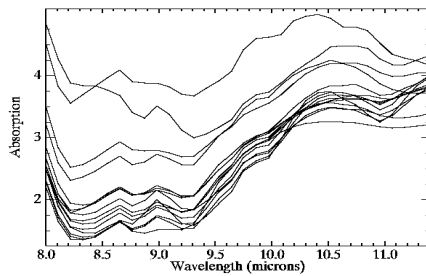


Figure 4: Selection of the resampled (TASI-600) and transformed ($\log_{10}(1/R)$) soil reflectance spectra in the TIR as they found input to the calibration modeling

Y	Spectral range	n	f	CALIBRATION			VALIDATION		
				R^2	RMSEC	expl. Y var.	R^2_{adj}	RMSEP	expl. Y var.
% clay	VNIR-SWIR	88	5	0.9	3.26	90.46 %	0.87	3.98	86.68 %
	TIR	88	4	0.93	2.42	93.04 %	0.87	3.23	87.29 %
	VNIR-SWIR-TIR	87	5	0.96	1.91	95.64 %	0.91	2.89	90.67 %
% sand	VNIR-SWIR	87	5	0.88	4.39	87.56 %	0.84	4.85	83.95 %
	TIR	88	3	0.951	3.2	95.15 %	0.947	3.5	94.72 %
	VNIR-SWIR-TIR	87	5	0.96	2.62	95.75 %	0.94	3.1	93.37 %
% OC	VNIR-SWIR	84	6	0.83	0.11	82.99 %	0.79	0.13	78.67 %
	TIR	83	7	0.84	0.11	83.63 %	0.75	0.14	75.41 %
	VNIR-SWIR-TIR	83	5	0.88	0.09	88.34 %	0.85	0.1	84.55 %

Table 1: Prediction modeling calibration and validation results (number of samples (n), number of model factors (f), correlation coefficient (R^2) and -adjusted (R^2_{adj}), root mean square error of calibration (RMSEC) and -prediction (RMSEP), explained Y-variance).

3.1 Clay content

Predicting the soil's clay content from the TIR spectral region, the model performed well using four factors. With a correlation coefficient of 0.93 (RMSEC = 2.42) in the calibration and 0.87 (RMSEP = 3.23) in the validation, explaining most of the Y-variance (93.04 % in the calibration and 87.29 % in the validation) the results for the 32 thermal infrared bands were better than for the VNIR-SWIR-model (111 bands) on 5 factors (table 1). Three samples, outstandingly rich in clay, have a strong leverage effect on the model. Two of these clay rich samples (55.0 % and 58.5 % clay) are among the additional vertosols samples, collected further south of the investigation area to stretch the clay content range. The very clay extreme sample (68.4 % clay) was taken within the study area from a dried out clay pan. The influence of these samples for the model was assessed as being positive, since excluding these samples would have caused a much higher factorial model ($f > 15$) to explain a similar amount of the Y-variance. Best results were achieved with using the VNIR-SWIR and the TIR spectral region simultaneously. A 5 factor model produced correlation coefficients of 0.96 (RMSEC = 1.91) for the calibration and 0.91 (RMSEP = 2.89) for the validation and explained 95.64 % and 90.67 % of the Y-variance, respectively (Figure 5).

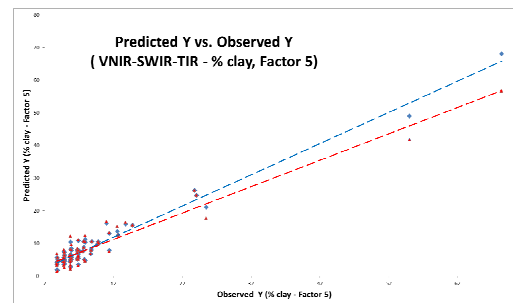


Figure 5: Predicted versus observed soil samples for the VNIR-SWIR-TIR-model on clay content using 5 factors.

3.2 Sand content

The models for predicting the soil's sand content revealed the best outcomes in this study. Especially the TIR showed promising results for this wavelength region. The model parameters were already stable after three factors. Here, sand was predicted with very high correlation coefficients ($R^2=0.951$ and $R^2_{adj}=0.947$) and with a high certainty for further

predictions (RMSEC = 3.2 and RMSEP = 3.5), explaining 95.13 % of the Y-variance in the calibration and 94.72 % in the validation, respectively (Figure 6). Predicting the sand content using the VNIR-SWIR and the TIR spectral region were inferior to using the TIR individually. The combined model needed two more factors to achieve similar results for the value of the correlation coefficients ($R^2=0.96$ and $R^2_{adj}=0.94$) and to explain a similar amount of Y-variance (95.75 % in the calibration and 93.57 % in the validation). However, the root mean square error was slightly improved to 2.62 (RMSEC) and 3.1 (RMSEP) using the additional 111 VNIR-SWIR bands.

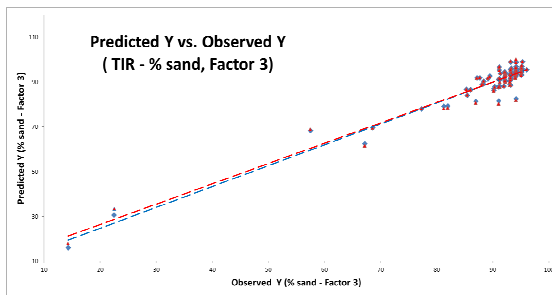


Figure 6: Predicted versus observed soil samples for the TIR-model on sand content using 3 factors.

3.3 Organic carbon content

Due to the relatively low organic carbon content in the soils of the investigation area (OC content with maximum of 1.68 % and minimum of 0.05 % among the collected soil samples) the models for this response variable performed poorer for its prediction compared to the texture variables for both the VNIR-SWIR and the TIR spectral signatures. Here, more outliers had to be removed from the data set, mainly those with outstandingly low content in organic carbon ($OC < 0.1$ %).

Models for both regions, the VNIR-SWIR and the TIR lead to similar results for predicting the OC from its spectral signatures. Whereas the VNIR-SWIR needed a less comprehensive model (6 factors), this was due to the fact that most of the organic soil components show their spectral activity within this wavelength range. But both models performed sufficiently well to show the inherent correlation between the response and predictor variables ($R^2 = 0.83$ in the VNIR-SWIR and 0.84 in the TIR with an RMSEC of 0.11).

Predicting the organic carbon content using the VNIR-SWIR and the TIR spectral region in combination, performed better (like for predicting clay) than with using the VNIR-SWIR- or the TIR model individually. With a five factor model the organic carbon content could be predicted with a correlation coefficient of 0.88 for the calibration and 0.85 for the validation. RMSEC (0.09) and RMSEP (0.1) were reduced and the explained calibration Y-variance (88.34 %) and

explained validation Y-variance (84.55 %) have both risen (Figure 7).

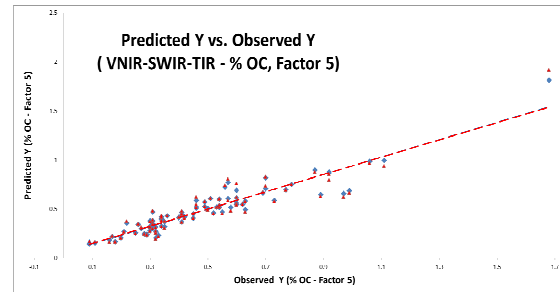


Figure 7: Predicted versus observed soil samples for the VNIR-SWIR-TIR-model on organic carbon content using 5 factors.

4. CONCLUSIONS

The study reveals that the prediction of the selected soil erosion relevant parameters is feasible using 32 bands within the thermal infrared emissivity spectra. These bands correspond to spectral specifications of a hyperspectral imaging sensor, the TASI-600.

All of the three selected soil parameters show good correlations with the spectral signatures ($R^2_{adj} = 0.87$ for % clay, 0.95 for % sand, and 0.75 for % OC). Due to its direct opto-physical relationships, the models for the TIR region performed best for the sand fraction with its high quartz content. Predicting clay and sand content could be done more accurately and reliably with the TIR than with using the VNIR-SWIR region. In most of the cases, modeling with the TIR could be realised with a reduced number of model factors, even the TIR provides less than a third of the VNIR-SWIR bands. In the case of organic carbon content, the individual VNIR-SWIR- and TIR models performed similarly and could be improved through simultaneously using both regions for the prediction modeling ($R^2_{adj} = 0.84$, RMSEP = 0.1). Combining the two spectral regions also improved the prediction of the clay content. However, to predict the sand content the performance of using the 32 TIR bands individually could not be improved by adding the 111 VNIR-SWIR bands.

Accordingly all of the spectral regions show their potential for a sufficient prediction for each of the soil erosion relevant parameters from the resampled laboratory spectral data. Nevertheless, with the focus on applying the prediction models to imaging spectroscopic data, we expect a surplus from the additional TIR bands. Dealing with limitations due to atmospheric influences and pixel inherent spectral mixture interactions, the use of TIR sensing will lead to a more flexible approach for quantifying soil parameters. In the case of predicting texture characteristics from very sandy soils (e.g. Mullewa) the TIR bands will promise more prediction accuracy, through their higher spectral contrast of their major mineral component, quartz. Taking into account the

limited range of OC content among the soil samples, the models show that the prediction of this soil parameter is basically feasible for both of the spectral regions, but would profit from a combination of them.

5. REFERENCES

Beard, J. S. 1976, *Vegetation Survey of Western Australia - Sheet 6 Murchison*, University of Western Australia Press, Nedlands, Western Australia.

Ben-Dor, E., Irons, J.R., Epema, G.F., 1999. Soil reflectance. *Remote Sensing for the Earth Sciences, Manual of Remote Sensing*. Wiley & Sons Inc., New York, pp. 111–188.

Brady, N.C., Weil, R.R., 2008. *The nature and properties of soils*. Prentice Hall, 14 edition.

Chabrilat, S., Goetz, A. F. H., Olsen, H. W., and Krosley, L. (2002). Use of hyperspectral images in the identification and mapping of expansive clay soils and the role of spatial resolution. *Remote Sens. Environ.* 82(2–3), 431–445.

Chang, C. and Laird, D.A., 2002. Near-Infrared reflectance spectroscopic analysis of soil C and N, *Soil Science* 167(2).

Cudahy, T.J., 2000. *Mapping Surface Mineralogy and Scattering Behaviour Using the Mid-infrared Airborne CO₂ Laser Spectrometer (MIRACO2LAS)*. Dissertation, Curtin University of Technology, Perth.

Clark, R.N., G.A. Swayze, A.J. Gallagher, T.V.V. King, and W.M. Calvin, 1993. *The U. S. Geological Survey, Digital Spectral Library: Version 1: 0.2 to 3.0 microns*, U.S. Geological Survey Open File Report 93-592, 1340 pages.

Eisele, A., Bachmann, M., Mueller, A., 2007. Capability to quantify pedo-chemical parameters using spectroscopic data of semi-arid soils in the Otjozondjupa region, Central Namibia. *Proceedings of the 5th EARSeL Workshop on Imaging Spectroscopy*. Bruges, Belgium, April 23-25 2007.

Hapke, 1993. *Theory of Reflectance and Emittance Spectroscopy*. Cambridge University Press, New York (1993).

Isbell, R.F. (1996). *The Australian Soil Classification*. CSIRO Publishing, Melbourne, Australia.

Martens, H., Næs, T., 1989. *Multivariate Calibration*. John Wiley and Sons, Chichester, p. 419.

McKenzie N, Henderson B, McDonald W (2002) *Monitoring soil change. Principles and practice for Australian conditions*. CSIRO Land and Water Technical Report 10/02

Nicodemus, F.E., (1965). Directional reflectance and emissivity of an opaque surface. *Applied Optics*, 4 (7), 767- 773.

Salisbury, J.W. and D’Aria, D.M. 1992. Emissivity of Terrestrial Materials in the 8-14mm Atmospheric Window. *Remote Sensing of Environment*, 42:83-106.

Viscarra Rossel, R.A., Walvoort, D.J.J., McBratney, A.B., Janik, L.J., Skjemstad, J.O., 2006. Visible, near infrared, mid infrared or combined diffuse reflectance spectroscopy for simultaneous assessment of various soil properties. *Geoderma* 131, 59–75.

Walkley, A., Black, I.A., 1934. An estimation of the Degtjareff method for determining soil organic matter and a proposed modification of the chromic acid titration method. *Soil Science* 37, 29–37.

6. ACKNOWLEDGEMENTS

A great Thank You goes to all the coauthors from CSIRO, METI/ERSDAC, and DAFWA for your great support.